

Advection of the image point in probabilistically-reconstructed phase spaces

Igor Shevchenko

National Oceanography Centre, European Way, Southampton, SO14 3ZH, UK

Abstract

Insufficient reference data is ubiquitous in data-driven computational fluid dynamics, as it is usually too expensive to compute or impossible to observe over long enough times needed for data-driven methods to properly operate out of the sampled range. Ultimately, the lack of data can significantly compromise the fidelity of results computed with data-driven methods or make the data-driven approach inapplicable. In order to challenge this problem, we propose a probabilistic reconstruction method which enriches the hyper-parameterisation approach with ideas underlying the probabilistic-evolutionary approach. We offer to use Advection of the image point (a hyper-parameterisation method) on data sampled from the joint probability distribution of the reference dataset. The idea is to blend together the simplicity of the hyper-parameterisation (HP) method with an extra source of reference data provided through sampling from the joint probability distribution.

The HP method has been tested on the sea surface temperature and surface relative vorticity computed with the global $1/4^\circ$ and $1/12^\circ$ resolution NEMO model. Our results show that the HP solution (the solution computed with the HP method) in the probabilistically-reconstructed and reduced (in terms of dimensionality) phase space at $1/4^\circ$ resolution is more accurate compared to the $1/4^\circ$ -solution computed with NEMO and it is also several orders of magnitude faster to compute than the $1/4^\circ$ -run. The proposed method shows encouraging results for the NEMO model and the potential for the use in other operational ocean and ocean-atmospheric models for both deterministic and probabilistic predictions. The method can also be used as a fast reanalysis in which the complex dynamics of a comprehensive ocean model is replaced with the HP solution, as well as a dynamic interpolation method

to stitch gaps in observational data.

Keywords: hyper-parameterization, NEMO ocean model, data-driven method, probabilistic reconstruction, phase space, state space, reanalysis, dynamic interpolation

1. Introduction

The data-driven paradigm is gradually gaining momentum in computational fluid dynamics by offering an alternative to the physics-driven approach in situations when there is no physics-based model for the studied phenomenon or it is too computationally-expensive to acquire data from the model (e.g. [1] and references therein). The data-driven approach includes a variety of methods, spreading across different fields (e.g. statistical modelling [2, 3], dynamical system reconstruction [4, 5, 6, 7], hybrid modelling [8, 9], probabilistic-evolutionary approach [10], etc.) In recent years, machine learning (ML) methods started to enrich the data-driven approach with artificial neural networks (e.g. [11, 12, 13, 14, 15, 16]) typically trained on reanalysis data or reference runs of physics-driven models. The majority of these ML methods are used for predictive modelling (e.g. [17, 18, 19]), while some, known as Interpretable ML, go beyond traditional ML predictions and try to improve our understanding of modelled phenomena (e.g. [20, 21]).

Being a powerful tool providing a wide spectrum of methods ranging from purely-data to physics-data driven, also known as hybrids, the data-driven approach typically suffers from the lack of reference data that can significantly compromise its fidelity or make it inapplicable. In order to help this problem, we offer a probabilistic reconstruction method which augments the hyper-parameterisation (HP) approach (e.g., [22, 8, 23, 24, 9]) with some ideas underlying the probabilistic-evolutionary approach [10]. More specifically, we propose to use Advection of the image point (a purely data-driven HP method working in phase space, also called state space) together with data sampled from the joint probability distribution of reference data so as to probabilistically reconstruct the reference phase space for the HP method and make it operable for short reference data records otherwise falling out of its range of applicability. The main difference between the proposed methodology and ML methods (based on artificial neural networks) is that: the former does not have the training phase (the calibration procedure of the HP method might be interpreted as such though), it uses phase spaces instead

of the physical space, respects the regional stability property, and relies on the unconventional calculation of directional vectors. The regional stability is defined as a property of the solution of a differential equation to permanently remain in a neighborhood of the phase space region if the initial condition is sufficiently close to that region. By the unconventional calculation of directional vectors we mean how the right hand side (RHS) in the HP method is calculated. Namely, we do not use a sequence of following each other states from the past (as conventional integrators) to calculate the RHS, but use the states neighboring the current state in the phase space.

The main advantages of the HP method in probabilistically-reconstructed phase spaces are the following:

- **Flexibility.** The method enables research situations involving HP of only some part/component of the ocean circulation: geographical part (ocean surface or deep layers, different basins, etc.), specific field (salinity, temperature, velocity, etc.), specific observations (drifter, satellites, etc.), or their combination. For example, one can use HP only for the ocean circulation and solve separately for the biochemical processes embedded into it (e.g. carbon cycle research);

- **Scalability.** HP offers a great resolution scalability and can be used to parametrise the effect of any high-resolution process into lower-resolution systems (e.g. mesoscales processes in larger-scale processes, sub-mesoscale processes in mesoscale-resolving/sub-mesoscale-permitting systems, etc.), and therefore it can be readily adopted by forecasting systems;

- **Alternative to parameterisations,** which can be used in comprehensive ocean models (NEMO, MITgcm, FESOM, etc.);

- **Fast generation of ensembles.** HP is well-suited for generating ensembles of solutions, which serve many purposes in ocean and atmospheric modelling;

- **HP as a tool for process studies.** HP allows one to study oceanic feedbacks on climate. In this case the ocean is fully under control; one can systematically change parameters and properties of the ocean circulation and find out their global consequences. Using HP one can uncover and understand internal links and feedbacks within the system, by replacing specific components with HP analogues.

Although, we consider the use of probabilistically-reconstructed phase spaces within the HP framework, its application is not bound to HP. For example, probabilistically-reconstructed reference datasets can be used within the context of other data-driven methods, as well as for training artificial neu-

ral networks, and for reconstruction of missing parts in observational data from different sources (drifters, weather stations, satellites, etc.)

2. The probabilistic reconstruction method: schematic and basics

The idea underlying the probabilistic reconstruction method is to calculate the joint probability distribution (JPD) for a given reference dataset and then sample reference data from this JPD instead of using the reference dataset itself. Hence, the JPD becomes an extra layer between the reference data and a data-driven method thus providing an extra source of reference data from the reference data distribution. It would be instructive to first look into the schematic of the proposed method (Fig. 1) for better understanding of its specifics and then consider the method in more detail.

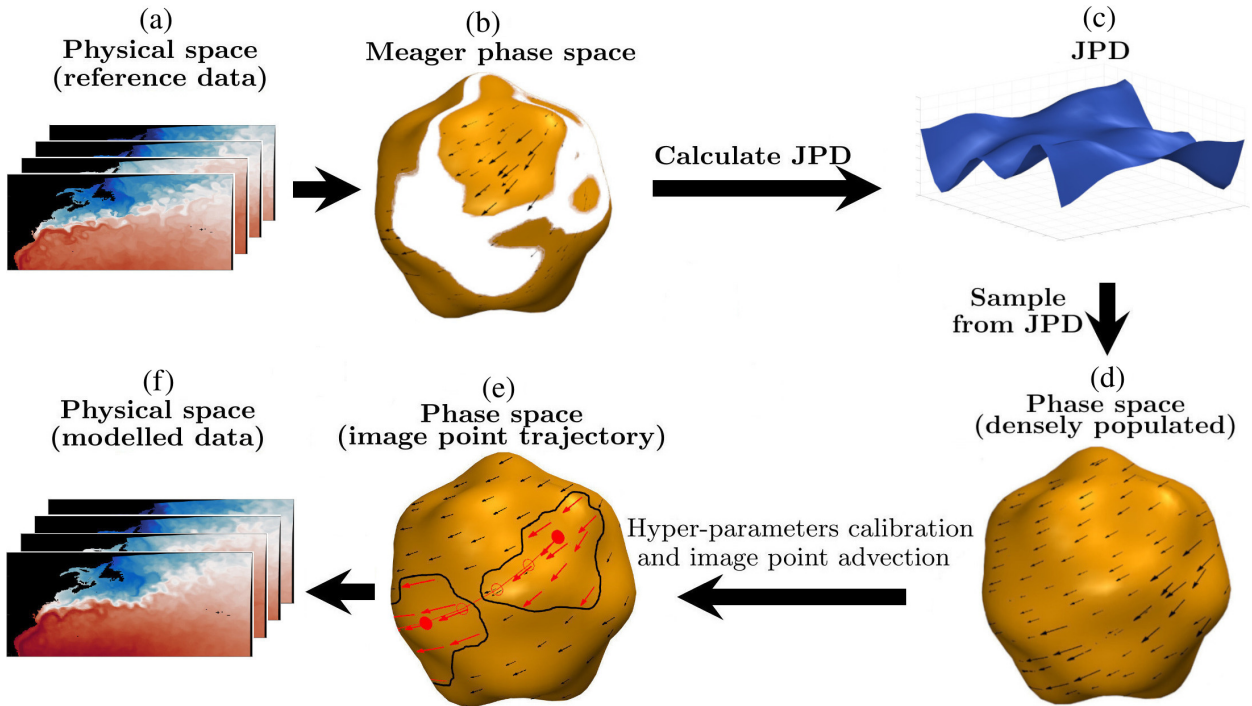


Figure 1: Schematic of the probabilistic reconstruction method.

(a) Reference data acquisition. The first step is to provide the method with reference data. Depending on the problem to solve, it can be numerical simulations, observations, or both. In our case it is sea surface temperature

(SST) computed with a global $1/12^\circ$ resolution ocean model NEMO and then interpolated onto a $1/4^\circ$ grid (Fig. 1a); SST is a scalar field defined on a cartesian grid. If observations are available then they can also be included in the reference dataset by simply adding them to the reference data record. In order to be consistent in space, observations must be on the same grid as the NEMO data; consistency in time is not required, as the proposed method does not use it.

(b) Reference phase space calculation. Before proceeding with the second step it would be helpful to remind the reader that a phase space (or state space) is an abstract mathematical space of all possible states of a physical system, while the physical space is typically defined as the actual three-dimensional space we all live in.

The second step is to get the reference phase space for the HP method called "Advection of the image point" [22, 24]; the reference phase space is shown as an orange blob in Fig. 1b. The latter needs states (which is SST itself) and directional vectors (time derivatives of SST, also referred to as tendencies), which are calculated from the reference data; different schemes can be used, we use the central finite difference in time. The tendencies are shown as black vectors in Fig. 1b, and the points they are attached to represent SST, which is a vector in the phase space, while it is a scalar field in the physical space.

The white spots (which we call voids) are regions of the phase space which lack data (usually, due to short reference records or unreliable observations). Typically, these voids is a reason for why data-driven methods cease to work on meager phase spaces.

(c) Joint Probability Distribution calculation. The third step is to calculate the joint probability distribution (JPD) from the reference data in phase space; it is shown as a blue surface in Fig. 1c for illustration purposes. In high-dimensional phase spaces (like the one used for SST) the JPD is a hyper-surface. It is important to remark that we calculate the JPD only for SST, while SST tendencies are computed in a different way explained below. The JPD for the reference SST is calculated globally, i.e. the whole reference dataset is used in the calculation.

The standard approach to calculate an approximation to the JPD is to use the histogram method. This method is based on the subdivision of the domain into hypercubes (bins) and count the number of states in every bin to compute the height of each column of the multidimensional histogram; the domain is a hypercube in the phase space of SST in our case, the phase

space dimension is equal to the number of grid points needed to approximate SST in the physical space. This method works well only in low-dimensional spaces, since the computer memory needed grows as the number of bins to the power of the space dimensions. Therefore, in high-dimensional spaces (like the one used for SST) computing a multidimensional histogram and keeping it in memory for further sampling is an unaffordable option.

In this study, we do not calculate the whole multi-dimensional histogram. Instead, we compute a coordinate-wise probability density function (PDF) for every component of the state (i.e. for every grid point of SST) and then use these PDFs to sample from the JPD; it gives us access to all necessary information for sampling at virtually no cost. Notice that these PDFs can be interpolated if there is not enough reference data to accurately approximate the PDFs.

(d) Sampling from JPD and calculation of probabilistically-reconstructed phase space. In the fourth step we sample SST from the JPD and then calculate SST tendencies by averaging reference SST tendencies over the neighborhood of sampled SST (Fig. 2). The localized calculation

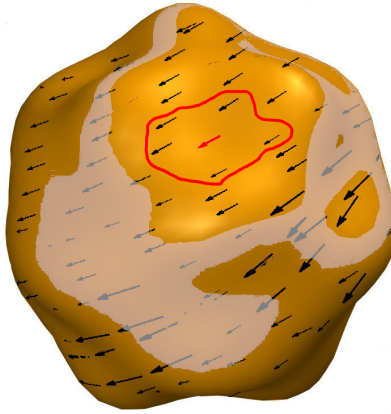


Figure 2: Shown is a schematic representation of the probabilistically-reconstructed phase space with the superimposed voids (grey regions). A new tendency (red vector) is computed as an average of reference tendencies (black vectors) in the neighborhood of sampled SST (red contour).

of tendencies allows to decrease the dimensionality of the JPD two times (as the JPD dimension for both SST and its tendencies is two times larger compared to the JPD only for SST) and thus make its calculation more efficient without compromising on accuracy. It is worth mentioning that tenden-

cies can also be computed in a probabilistic way from a local JPD which is constructed based on the information from the neighborhood of the new tendency (red contour in Fig. 2), but this method is slower than the one used in this study.

In order to sample from the JPD we use the inverse transform sampling method [25]. We have also tried the rejection sampling but did not gain that much of a difference in its favour; a sampling method based on a reverse-time stochastic differential equation [26] might be another option instead of the inverse transform sampling. Sampling from the JPD allows us to probabilistically reconstruct the originally sparsely-populated reference phase space by filling it with new states and directional vectors (tendencies) needed to advect the image point (Fig. 1d). Note that the probabilistically-reconstructed reference data can be used not only in the HP method, but in other data-driven methods which suffer lack of data.

We would like to draw the reader's attention to the fact that the new states generated by sampling from the JPD does not mean new reference states (i.e. the states generated by the underlying reference model, it is the NEMO model in our case), since sampling from the JPD cannot guarantee that sampled states are reference states, and the HP dynamics in probabilistically-reconstructed phase spaces cannot guaranteed it either.

For a more detailed discussion on how the sampling procedure calculates a new state, we consider a two-dimensional case (i.e. a set of points in an XY-plane) for simplicity. In this case we have two coordinate-wise PDFs (one for each dimension). Sampling starts from computing the PDF for the first dimension and its corresponding CDF. Next, we draw a random number $r_1 \in U[0, 1]$, with $U[0, 1]$ being a uniform distribution in the unit interval, and find $x_1(r_1)$ with the inverse transform sampling method, where $x_1(r_1)$ is the first coordinate of the new state. In order to calculate the second coordinate of the new state, we compute the PDF for the second dimension given $x_1(r_1)$ and its CDF. Then, we draw another random $r_2 \in U[0, 1]$ and compute $x_2(r_2)$, which is the second coordinate of the new state. In this way we can sample as many states as we need from the reference JPD.

It is also important to note that SST and its tendencies in the probabilistically-reconstructed phase space are not ordered in time. This is the moment when we need Advection of the image point to compute a trajectory (solution), i.e to order those points in time.

(e) Advection of the image point in probabilistically-reconstructed phase space. In the fifth step, the probabilistically-reconstructed phase

space is used by Advection of the image point to calculate the trajectory (red line in Fig. 1e). For the reader’s convenience, we briefly describe how Advection of the image point works. This method falls into the category of data-driven methods from the hyper-parametersation (HP) class which takes advantage of working in phase spaces, as opposed to the conventional methods operating in the physical space. The method has been tested on both idealized and comprehensive ocean models (two-layer quasi-geostrophic model in a channel and MITgcm in the North Atlantic configuration) and showed significant improvements of the HP solution toward the reference one [22, 24]. The HP approach currently umbrellas five different methods (ranging from purely data-driven to hybrids, which combine the data- and physics-driven paradigms). Another striking feature of the HP approach is that its measure of goodness is how close the HP solution is to the reference phase space. To put it another way, the HP approach matches phase spaces (the reference phase space and the phase space where the HP solution evolves), whereas conventional methods match individual trajectories. This measure allows the HP solution to evolve in the neighborhood of the reference phase space, and therefore reproduce the flow dynamics which is very similar to the reference one.

The idea behind Advection of the image point (which we refer to as the HP method in what follows) is to use reference data, say $\mathbf{x} \in \mathbb{R}^n$, and the following differential equation

$$\frac{d\mathbf{y}}{dt} = \frac{1}{M} \sum_{j \in \mathcal{U}_J} \mathbf{F}(\mathbf{x}_j) + \eta \left(\frac{1}{N} \sum_{i \in \mathcal{U}_I} \mathbf{x}_i - \mathbf{y}(t) \right), \quad \mathbf{y}(t_0) = \mathbf{y}_0, \quad (1)$$

to describe the evolution of the image point, $\mathbf{y} \in \mathbb{R}^n$, in the phase space of reference data. In the context of this work, $\mathbf{x}(t)$ is the probabilistically-reconstructed SST, and $\mathbf{y}(t)$ is the HP solution computed in the probabilistically-reconstructed phase space, and η is the nudging strength. The neighbourhood of $\mathbf{y}(t)$ is denoted as $\mathcal{U}(\mathbf{y}(t))$, \mathcal{U}_I and \mathcal{U}_J are the sets of timesteps indexing the discrete reference solution \mathbf{x} in $\mathcal{U}(\mathbf{y}(t))$. Although the method allows to use different sets of reference tendencies $\mathbf{F}(\mathbf{x}_j)$ and points \mathbf{x}_i , we set $M = N$ and $\mathcal{U}_I = \mathcal{U}_J$ in this study.

In a nutshell, the actual dynamics is given by the observed reference tendency $\frac{1}{M} \sum_{j \in \mathcal{U}_J} \mathbf{F}(\mathbf{x}_j)$ the imperfect reconstruction of which from the reference data is compensated by nudging towards the observed reference

state $\frac{1}{N} \sum_{i \in \mathcal{U}_I} \mathbf{x}_i$ in the probabilistically-reconstructed phase space. Note that the neighbourhood is computed as the average over M (and N for the nudging term) nearest, in l_2 norm, to the solution $\mathbf{y}(t)$ points. The choice of the norm and the way the neighborhood $\mathcal{U}(\mathbf{y}(t))$ is calculated is not limited to those used in this study, and can vary depending on what is needed. Our choice is, probably, the simplest, but it serves well the purpose of this work. We dub the set of parameters $\{M, N, \eta\}$ hyper-parameters. The hyper-parameters can be set based on the chosen metric and available data, we will return to their choice later. The interested reader is referred to [22, 24] for a more detailed discussion of the method.

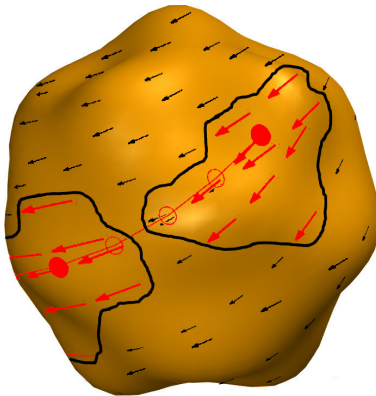


Figure 3: Shown is a sketch of the probabilistically-reconstructed reference phase space (orange blob), vectors $\mathbf{F}(\mathbf{x}_i)$ (black arrows) pointing out from points \mathbf{x}_i . For the HP method all these points is a cloud of points which are not ordered in time. The HP solution $\mathbf{y}(t)$ is shown as a red trajectory, and the neighborhood $\mathcal{U}(\mathbf{y}(t))$ is the black contour surrounding the red dot, which is the HP solution $\mathbf{y}(t)$ at time t . The red vectors (and also every point they are attached to) within the neighborhood are the N reference fields \mathbf{x}_i , $i \in \mathcal{U}_I$ (and M reference tendencies $\mathbf{F}(\mathbf{x}_i)$) nearest, in l_2 -norm, to the HP solution $\mathbf{y}(t)$. We assume that $\mathcal{U}_I = \mathcal{U}_J$ and $M = N$, but the method is not bound to this particular choice.

The characteristic feature of the HP method is that it looks at the reference dataset as being a cloud of points which are not ordered in time. This is why we write \mathbf{x}_i and $\mathbf{F}(\mathbf{x}_j)$ instead of $\mathbf{x}(t)$ and $\mathbf{F}(\mathbf{x}(t))$ in equation (1). At every time step, the HP method takes N nearest points \mathbf{x}_i (and M tendencies $\mathbf{F}(\mathbf{x}_j)$) to the solution $\mathbf{y}(t)$ points (Fig. 3). Thus, the HP method never runs out of reference data, as a set of nearest points to the HP solution $\mathbf{y}(t)$ can always be found. The main advantage of using the HP method in

probabilistically-reconstructed phase spaces is that the data for the method is sampled from the same distribution as the reference data itself.

It is important to differentiate between the reference data set and the reference phase space. The former is the skeleton of the latter, i.e. the reference data set is a set of states used in the proposed methodology to discover the reference phase space through the use of the HP method in the probabilistically-reconstructed phase space.

Calibration of hyper-parameters. The HP method has hyper-parameters $\{M, N, \eta\}$ which should be properly set to address the problem at hand. In order to calibrate these hyper-parameters we define a measure of discrepancy of two clouds of points, say A and B , as follows

$$\text{Di}(A, B) := \|A - \{\widehat{\min} d(a_i, B)\}_{1 \leq i \leq |A|}\|_2 / \|A\|_2, \quad (2)$$

where d is the Euclidean distance between the i -th point in A and a point in B ; $|\cdot|$ is the number of points in the cloud (it is assumed that $|A| = |B|$). The cloud A represents the reference data, while the cloud B is the HP solution computed in the probabilistically-reconstructed phase space; the clouds are not supposed to have any order defined on them.

It is important to remark that the $\widehat{\min}$ in (2) is excluding, i.e. once the minimum between a pair (a_i, b_j) has been found, the point b_j is excluded from B (to avoid multiple counting) and is then used in comparison with element a_i . In other words, $\widehat{\min}$ does not return the minimum distance between a_i and B per se, it returns the element b_j that delivers this minimum distance. Also note that the choice of this measure of discrepancy reflects the measure of goodness used for the HP method (namely, the proximity of the phase space (where HP solution evolves) to the reference phase space, or more accurately to the probabilistically-reconstructed reference phase space). The calibration procedure consists of minimizing the discrepancy on the space of hyper-parameters; the smaller the discrepancy is, the closer the clouds are to each other. We would like to remind the reader again that the HP method tries to match phase spaces (not individual trajectories), and this is why the calibration of hyper-parameters makes itself useful.

(f) Evolution in physical space. The fifth step is to compute the modelled solution back in the physical space (Fig. 1f). In this study, the solution computed with the HP method is reshaped from a vector (used in the phase space) into a scalar field, which is used to present fields in the physical space.

3. The probabilistic reconstruction method in action

In this section we apply the proposed method to Chua's circuit to demonstrate how it works in a low-dimensional phase space and then consider its application in the context of the global NEMO model.

3.1. Chua's circuit

As a minimum working example, we consider Chua's circuit and demonstrate in more detail how the method works. Chua's circuit [27] is given by the following system of equations:

$$\frac{d\mathbf{x}}{dt} = \mathbf{F}(\mathbf{x}(t)), \quad \mathbf{F} := \begin{pmatrix} \alpha(y - ax^3 - cx) \\ x - y + z \\ -\beta y - \gamma z \end{pmatrix}, \quad (3)$$

with $\mathbf{x}(t) = (x(t), y(t), z(t))$, and $\alpha = 10$, $\beta = 15$, $\gamma = 0.01$, $a = 0.1$, $c = -0.2$. As an initial condition, we take $\mathbf{x}(t_0) = (1, 0, 0)$ so that the solution is close to the attractor. Note that the solution $\mathbf{x}(t)$ at time t (being voltages across the capacitors and the current through the coil) is in the physical space, while the whole evolution of the solution (together with the time derivatives of the solution) is in the phase space.

Reference data acquisition. Within the context of Chua's circuit, the reference data for the HP method is the solution $\mathbf{x}(t)$ and its tendencies $\mathbf{F}(\mathbf{x}(t))$. In order to get the reference data we integrate the Chua system (3) over time $t \in [0, 100]$ and save the solution.

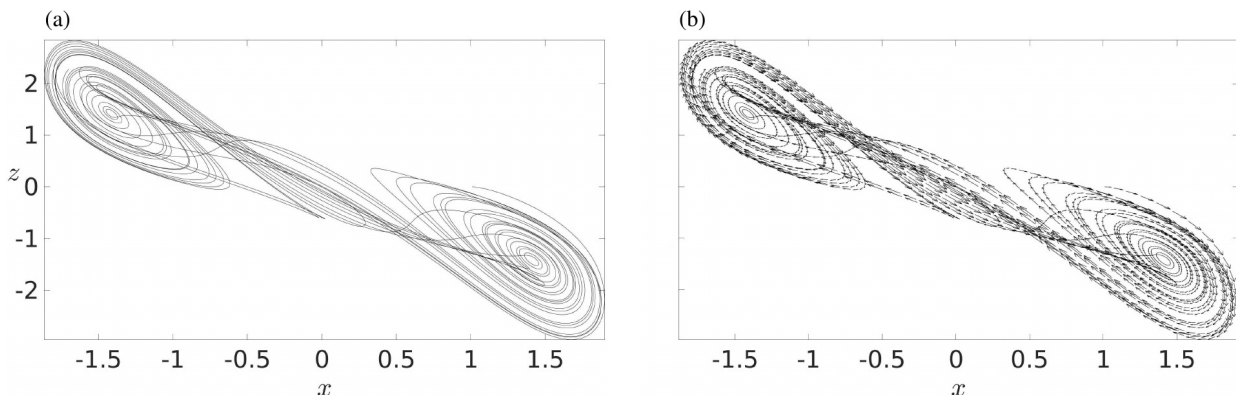


Figure 4: Shown is (a) the solution of Chua's system $\mathbf{x}(t)$ and (b) the corresponding vector field $\mathbf{F}(\mathbf{x}(t))$ for $t = [0, 100]$.

Then, the tendencies are computed by differentiating $\mathbf{x}(t)$; we use the central finite difference in time (Fig. 4). Instead of differentiating the solution, one can use the right hand side, but we recommend against doing that, as the right hand side is usually unavailable for numerical simulations and observations. Note that instead of or in combination with the numerical solution, one can also use observations. In this case, one should form a new dataset $\widehat{\mathbf{x}} = \{\mathbf{x}(t), \mathbf{x}_o(t)\}$, which includes both the solution $\mathbf{x}(t)$ and observations $\mathbf{x}_o(t)$.

Calculation of JPD and sampling from JPD. The JPD of the reference solution $\mathbf{x}(t)$ and reference tendencies $\mathbf{F}(\mathbf{x}(t))$ are calculated as described above. In order to make sure that sampling from the JPD is accurate enough for further use, we compare the reference PDF (computed from the reference dataset) and the reconstructed PDF (computed from the data sampled from the JPD). As seen in Fig. 5, the reconstructed PDF (blue) is an accurate approximation to the reference PDF (black); the reconstructed PDF can be calculated more accurately, but it is not required for the purpose of this study.

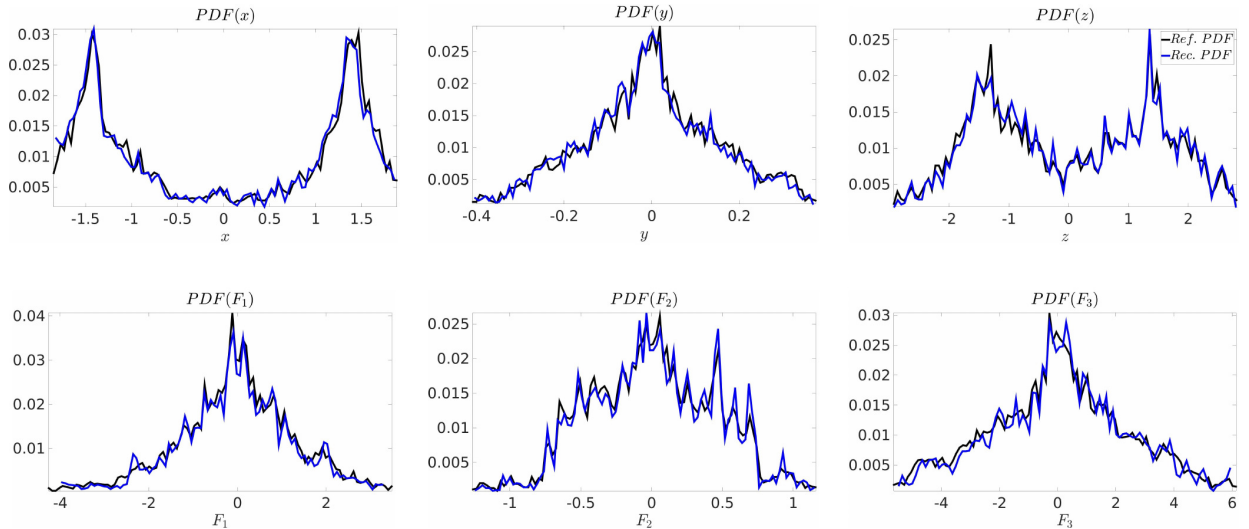


Figure 5: Shown is the coordinate-wise reference PDF (black) and reconstructed PDF (blue) for the solution of Chua’s system (top row) and for the corresponding vector field (bottom row). Note that the reconstructed PDF is an accurate approximation to the reference PDF.

The next step is to sample from the JPD to probabilistically reconstruct the reference phase space for the HP method. We use the same amount of

reference data as before, but harvest twice as much from the JPD (Figs. 6,7).
 The results clearly demonstrate the high quality of the probabilistically-

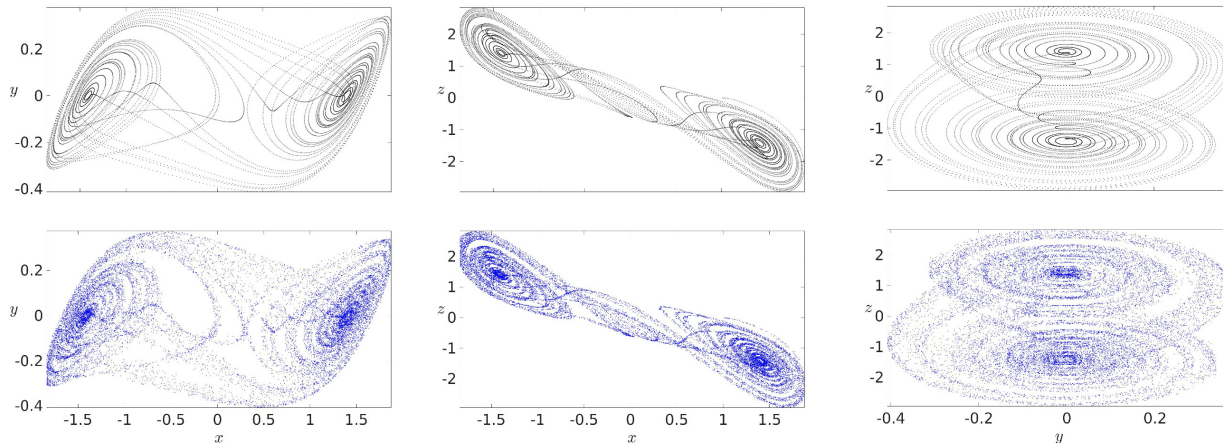


Figure 6: Shown are different projections of the reference solution (top row) and its reconstruction from the JPD (bottom row). The reconstructed data not only reproduces the reference one but, more importantly, densifies the phase space by adding new points, as we sampled twice as much points from the JPD compared with the reference data.

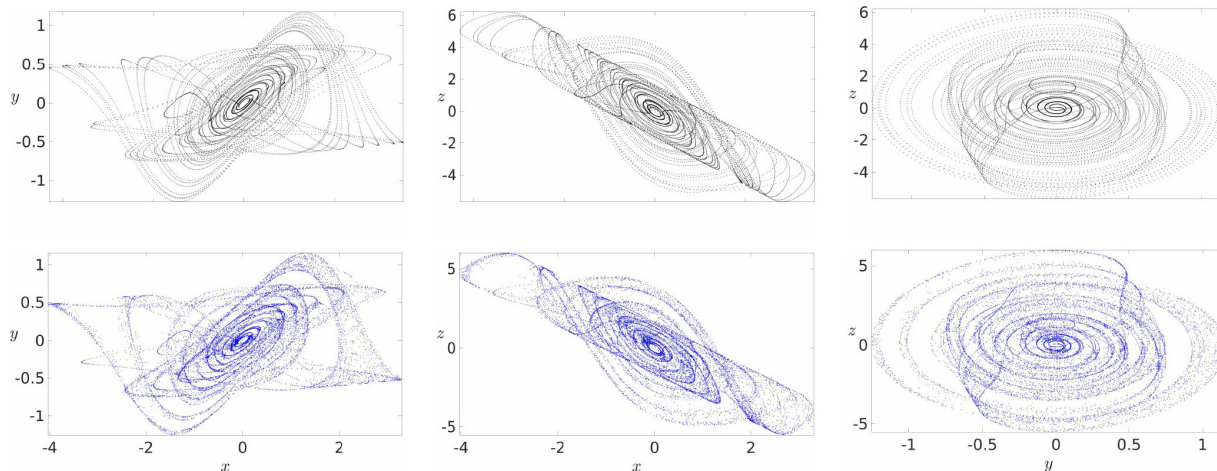


Figure 7: The same as in Fig. 6, but for the tendencies. The tendencies are not sampled directly from the JPD but are computed locally in the neighbourhood of the sampled solution.

reconstructed data, and that it covers a larger phase space compared with the reference one.

3.2. Calibration of hyper-parameters

The calibration procedure consists of minimizing $\text{Di}(A, B)$ in the space of hyper-parameters M , N , and η . One can opt for engaging a full-blown optimization to find the optimum solution. However, for the purpose of this study, we set $M = N = 5$ and search for $\eta \in [0, 1]$ that minimizes $\text{Di}(A, B)$. We have found that $\eta = 0.235$ gives a solution with low discrepancy.

In order to demonstrate that the proposed method can gain from using the probabilistically-reconstructed phase space, we compare it with the HP method run on the reference dataset (Fig. 8).

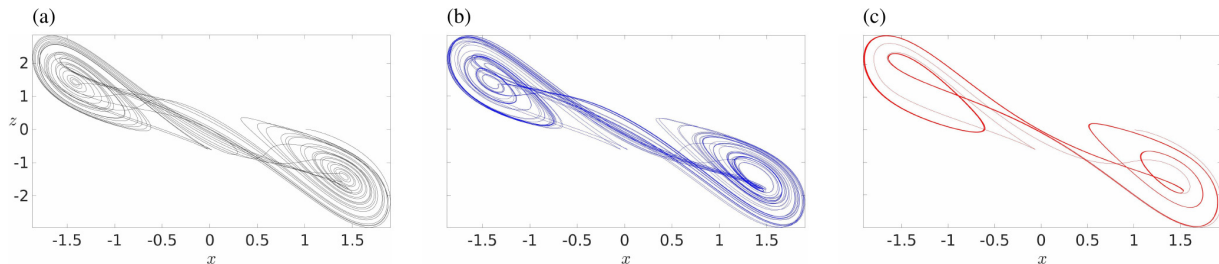


Figure 8: Shown are (a) the reference solution, (b) HP solution computed in the probabilistically-reconstructed reference phase space, and (c) HP solution computed in the reference phase space (no probabilistic reconstruction used); both HP solutions are computed for $M = N = 5$ and $\eta = 0.235$. The HP solution computed in the probabilistically-reconstructed reference phase space is much more developed compared with the HP solution computed in the reference phase space. Note that both HP solutions run for $t \in [0, 200]$, i.e. 50% of the time out of the reference sample.

As seen in Fig. 8b, the HP solution computed in the probabilistically-reconstructed phase space is very-well developed on the attractor compared with the HP solution computed on the reference dataset (Fig. 8c), which remains bounded to a very narrow band because of lack of data. All these results give an extra layer of confidence that the proposed method has strong potential for the use in more sophisticated models which we consider in the next section.

3.3. Corrupted reference data

Corrupted reference data is ubiquitous in the realm of data-driven methods. Reference data sets lacking states in the phase space or having vast voids (regions of no data) can significantly influence the accuracy of data-driven methods or make them inapplicable. Therefore, it is instructive to

study what happens when the reference data is damaged. As an example, we consider three different cases of the reference phase space corrupted with: (1) randomly-missed states, (2) gaps, and (3) cuts (Fig. 9). In all cases, sampling from the JPD reconstructs the phase space up to the extent, which is enough for the HP method to work. In the first case, sampling from the JPD densifies the attractor well (top subplot in Fig. 9b). In the second and third cases, however, there are still some voids in the reconstructed phase space (middle and bottom subplots in Fig. 9b) which cannot be completely filled in by sampling from the JPD, but the HP method does reproduce the dynamics on the attractor (similar to the reference one) nonetheless.

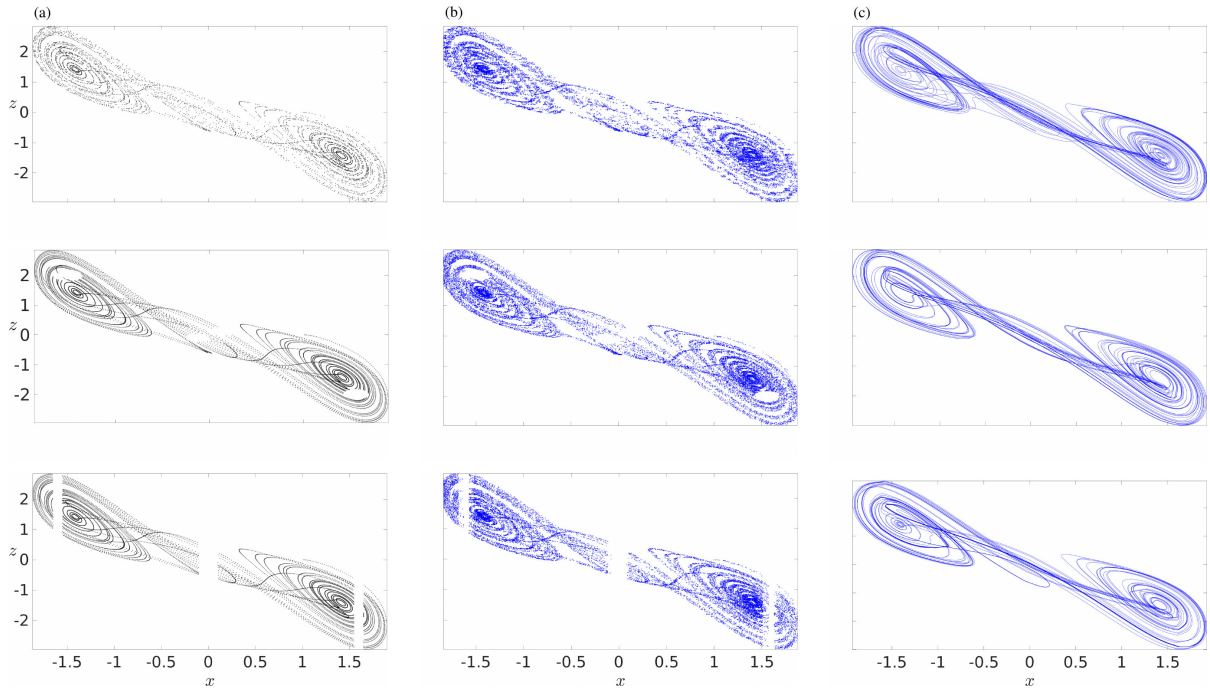


Figure 9: Shown are (a) reference data sets with different level of damage (top – (1) 50% of randomly-chosen states has been removed from the original reference data shown in Fig. 8a, middle – (2) original reference data with gaps, bottom – (3) original reference data with three cuts); (b) phase spaces probabilistically-reconstructed from the corresponding corrupted reference data sets; (c) HP solutions computed in the probabilistically-reconstructed phase spaces. In all cases, the HP method can reproduce the solution on the attractor even when sampling from the JPD cannot completely repair the damage. Note that for the HP method we use $\eta = 0.003$ for cases (1) and (2), and $\eta = 0.051$ for case (3).

The ability of the HP method to work in corrupted phase spaces can be exploited as a fast reanalysis method in which the complex dynamics of a comprehensive ocean model is replaced with the HP solution. The method can be thought of as a dynamic interpolation which can stitch gaps in observational data with the HP dynamics.

3.4. NEMO model

The output of the global $1/4^\circ$ (ORCA025-N4001) and $1/12^\circ$ (ORCA0083-N006) resolution NEMO model is used in this study. The reference solution is the 5-day mean sea surface temperature (SST) and surface relative vorticity (SRV) in the North Atlantic region $[-83^\circ W, -20^\circ W] \times [27^\circ N, 55^\circ N]$ over the period of 1979-1993; the period of 1994-2007 is used for validation to check how the HP method performs. The reference solution is interpolated from the $1/12^\circ$ -grid onto the $1/4^\circ$ grid. The lower-resolution $1/4^\circ$ -solution from ORCA025-N4001 simulation (we call it the modelled solution) is used for comparison with the HP solution.

In order to calibrate the hyper-parameters we take $M = N = 5$ and minimize $\text{Di}(A, B)$ with respect to η . We have found that $\eta = 0.01$ gives a low discrepancy. After setting up the hyper-parameters, we compute a probabilistically-reconstructed phase space by sampling twice as much compared to the reference record length (Fig. 10).

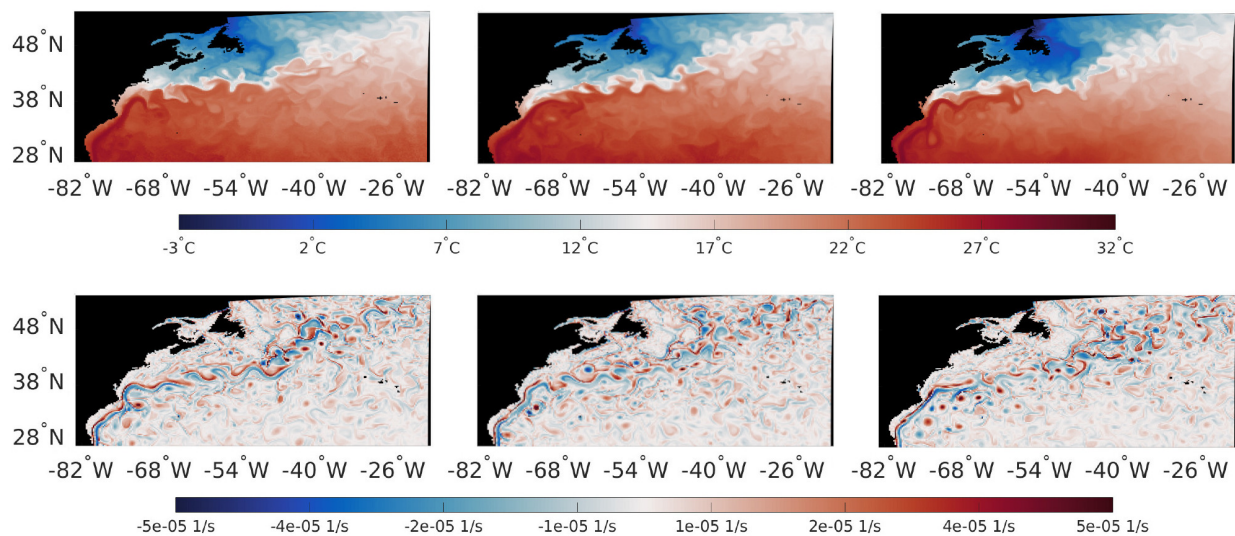


Figure 10: Shown are typical SST (top row) and SRV (bottom row) fields sampled from the reference JPD.

The dimensionality of the probabilistically-reconstructed space is $n \approx 30000$. One can run the HP method in the high-dimensional phase space, but in this work we further reduce it down to $m = 200$ by using the EOF-PC decomposition [28]. It results in a two-order of magnitude reduction compared with the original dimension; note that the 200 leading EOFs capture

99% of the total SST variance and 60% of the total SRV variance. We compute the EOF-PC decomposition of SST and SRV separately. However, it can be computed for both if one needs to model these fields together.

The space of PCs (let it be denoted as \mathbf{x}) can be regarded as a reduced version of the probabilistically-reconstructed phase space. Given this reduced space, one can reconstruct a dynamical system governing the reduced dynamics of observed reference data, as we did in [23]. In this study, we use a different idea: the dynamics of PCs is modelled in the reduced space with the HP method directly and then the HP solution is projected back into the full-dimensional probabilistically-reconstructed phase space.

In the reduced phase space, equation (1) reads as

$$\frac{d\mathbf{z}}{dt} = \frac{1}{M} \sum_{j \in \mathcal{U}_J} \mathbf{F}(\mathbf{x}_j) + \eta \left(\frac{1}{N} \sum_{i \in \mathcal{U}_I} \mathbf{x}_i - \mathbf{z}(t) \right), \quad \mathbf{z}(t_0) = \mathbf{z}_0, \quad (4)$$

where \mathcal{U}_I and \mathcal{U}_J are the sets of timesteps indexing the discrete reference solution \mathbf{x} in the neighbourhood of $\mathbf{z}(t)$. The only difference of (4) compared with equation (1) is that \mathbf{x} does not represent the reference solution (it would be SST or SRV in this case) but the PCs. Having solved equation (4), we approximate the HP solution, $\mathbf{y}(t)$, in the probabilistically-reconstructed phase space by using the leading EOF-PC pairs as follows:

$$\mathbf{y}(t) \approx \sum_{i=1}^m z_i(t) \mathbf{E}_i, \quad (5)$$

with \mathbf{E}_i and z_i being the i -th EOF and PC (computed with the HP method in the reduced space), respectively. Thus, solution $\mathbf{y}(t)$ is the SST (or SRV) computed in the full-dimensional probabilistically-reconstructed phase space.

We report the results in Fig. 11 which clearly shows that the HP solution (Fig. 11b) much better represents the Gulf Stream than the modelled solution (Fig. 11c). These results are also confirmed in Fig. 12. Namely, the difference between the time mean of the reference solution and HP solution is much smaller (Fig. 12a) than that of the modelled solution (Fig. 12b). The root mean square error for the HP solution (Fig. 12c) is also much lower than the one of the modelled solution (Fig. 12d). The time mean energy spectral density of the HP solution is closer to the reference than that of the modelled solution over the whole range of wave numbers (Fig. 12e, compare the blue and magenta graphs with the black one), and this difference is even more pronounced for SRV (Fig. 14e).

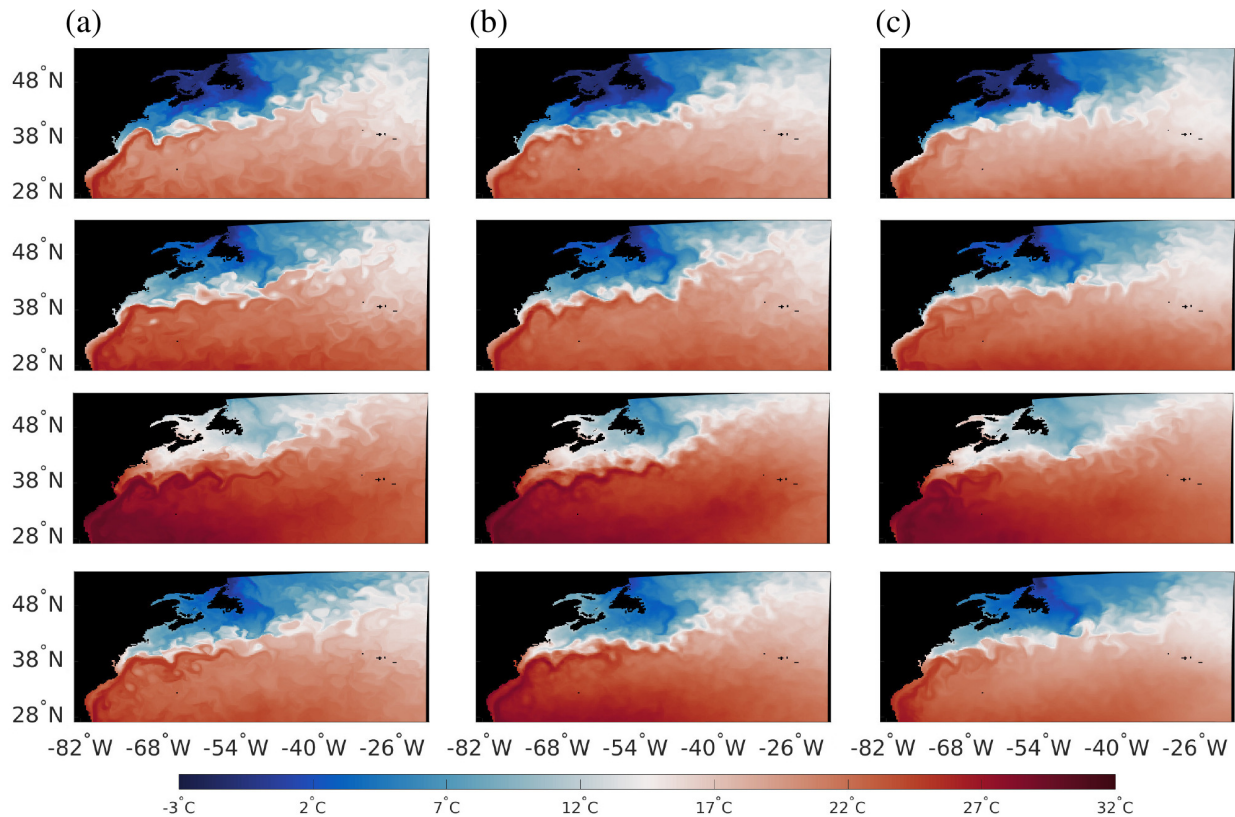


Figure 11: Shown are typical SST snapshots at $1/4^\circ$ resolution for (a) the reference solution, (b) HP solution, and (c) modelled solution. The HP solution significantly better represents the Gulf Stream compared with the modelled solution.

More insights about how the HP solution differs from the modelled solution can be seen in the SRV fields (Fig. 13). The Gulf Stream computed with the HP method (Fig. 13b) is much stronger than the one computed with the $1/4^\circ$ model (Fig. 13c). Moreover, the HP solution is teemed with vortices (like the reference one), while the vortex dynamics is significantly inhibited in the modelled solution as it is also reflected by the error plots in Fig. 14, as well as by the time mean energy spectral density, denoted as $\langle ESD \rangle$. The latter is more sensitive to the number of EOFs compared with SST, i.e. the more EOFs are used, the more accurate the $\langle ESD \rangle$ is. It is because SRV fields contain much more small-scale features (compared with SST), which therefore require more EOFs to be accurately represented. Doubling the number of PCs ($m = 400$) results in a more pronounced Gulf Stream dynam-

ics and larger population of vortices (Fig. 13), as well as in a more accurate representation of $\langle ESD \rangle$ (Fig. 14e). However, its contribution to the time mean flow and the root mean square error is small (not shown).

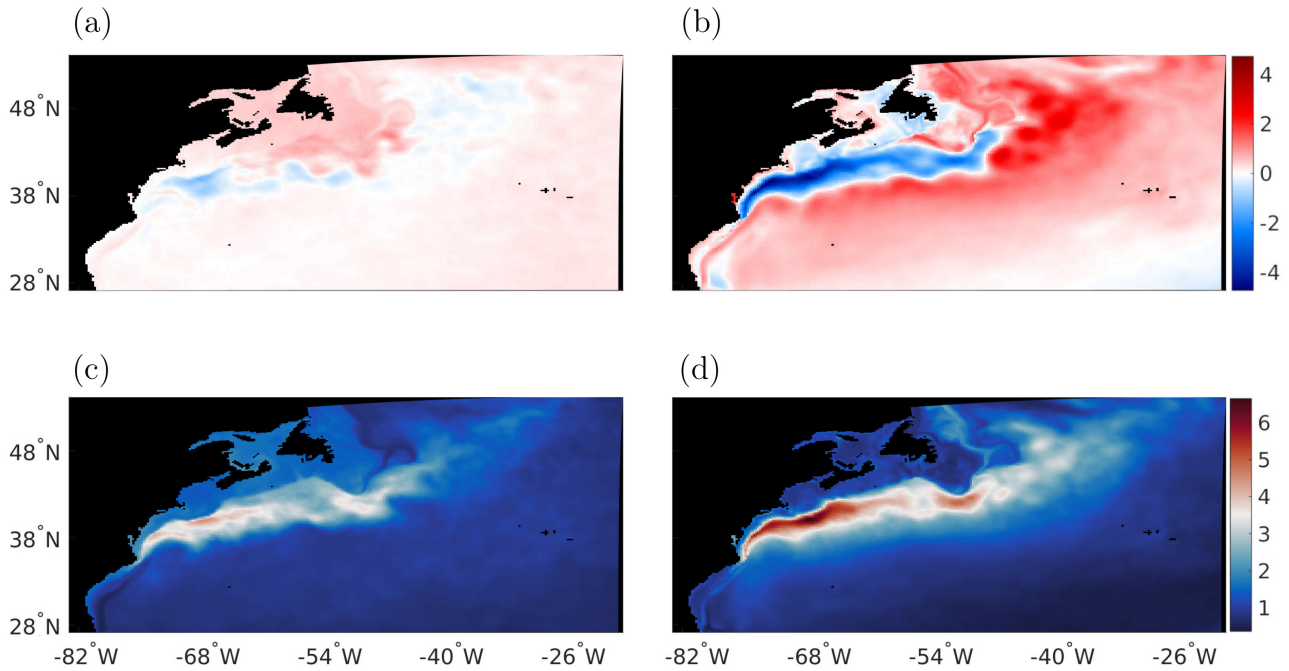


Figure 12: Shown are (a) difference between the time mean reference SST and HP solution, (b) difference between the time mean reference and modelled SST, (c) root mean square error between the reference SST and HP solution, (d) root mean square error between the reference and modelled SST, (e) the natural logarithm of the time mean energy spectral density $\langle ESD \rangle$ vs the magnitude of the wave vector \mathbf{k} . We use $m = 200$ in the EOF-PC decomposition for (a)-(d). The $\langle ESD \rangle$ of the HP solution (red and magenta) is closer to the reference (black) than that of the modelled solution (blue). Note that $\langle ESD \rangle$ for $m = 200$ (red) and $m = 400$ (blue) are almost the same, as adding more EOFs does not contribute much to the accuracy of SST. For illustrative purposes, we apply a locally estimated scatterplot smoothing (also known as a Savitzky-Golay filter) to smooth the ESD [29].

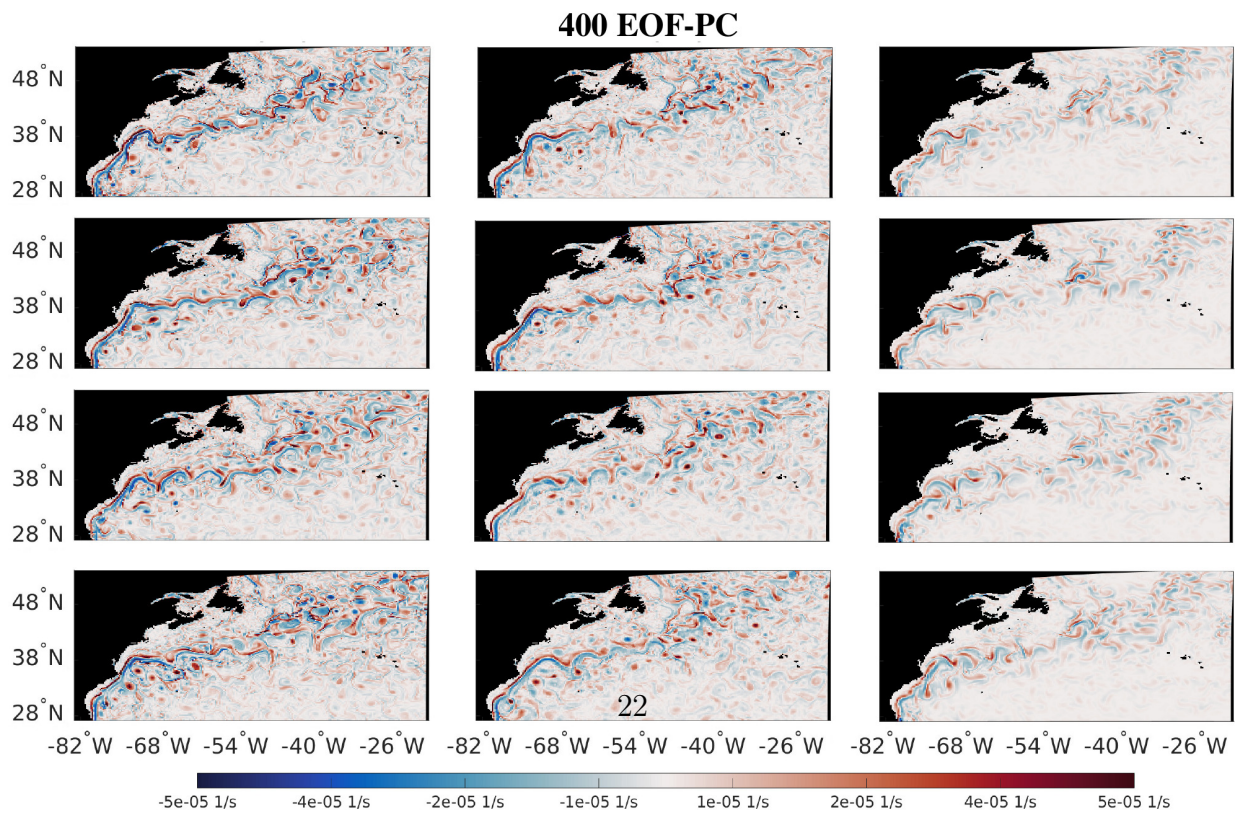
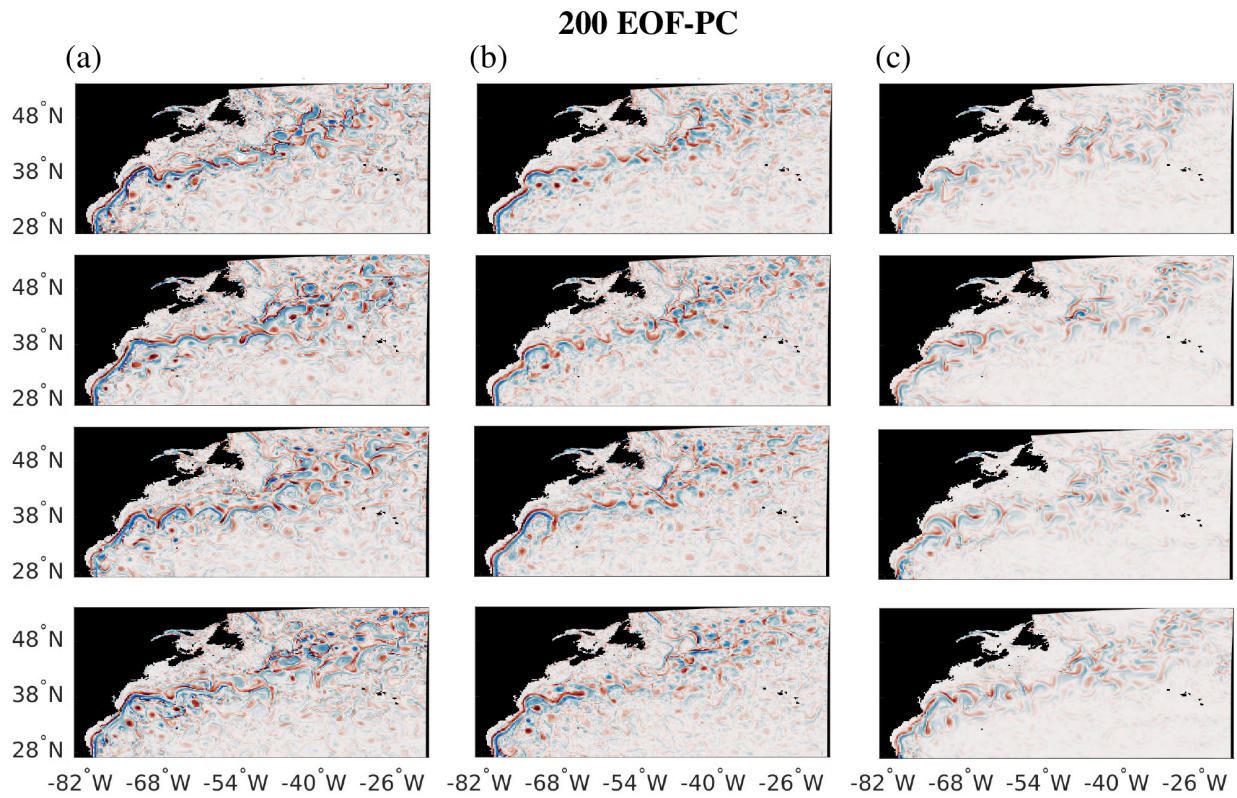


Figure 13: The same as in Fig. 12 but for SRV ($m = 200$ and $m = 400$).

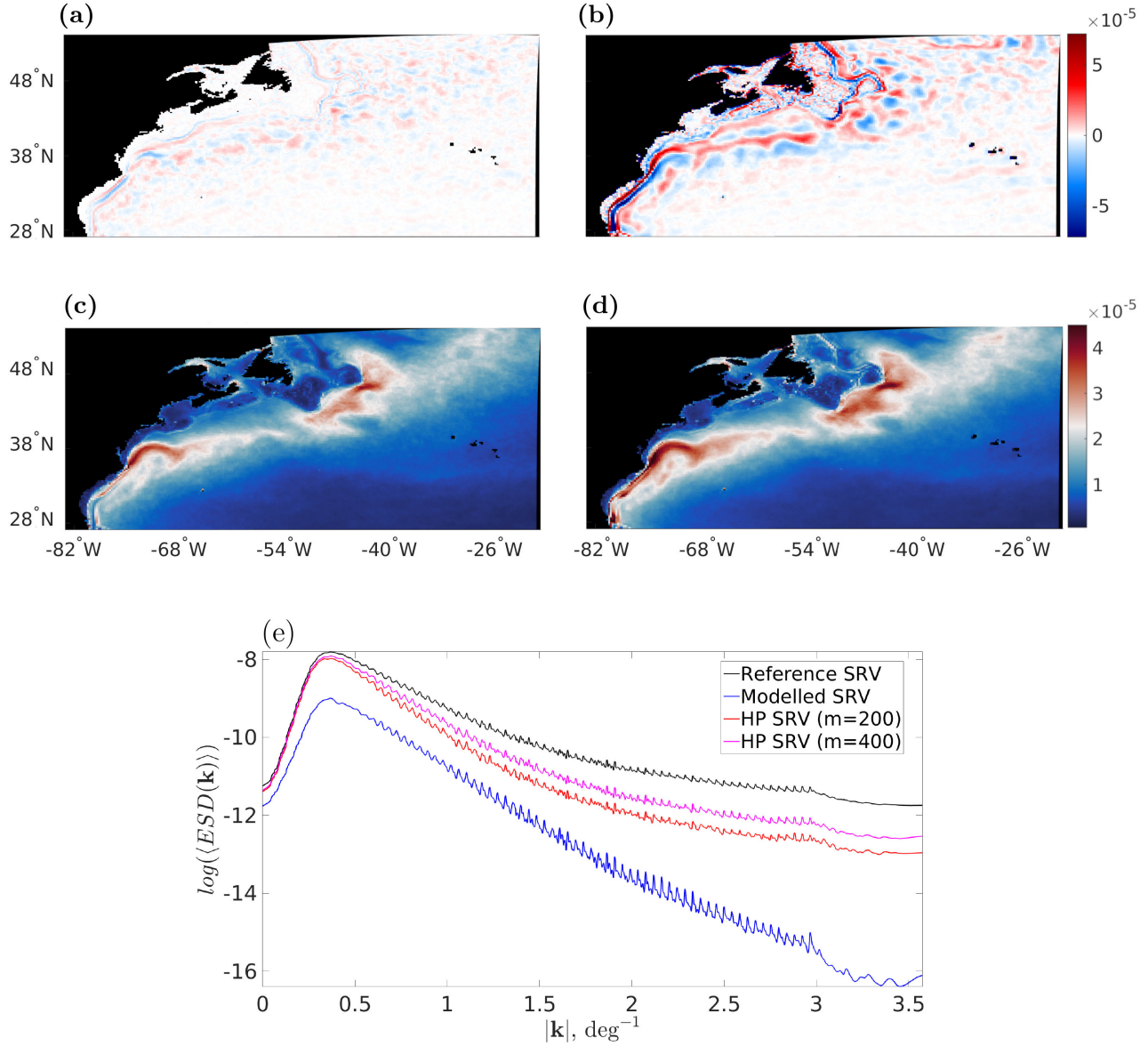


Figure 14: The same as in Fig. 12 but for SRV. Note that adding more EOFs makes the time mean energy spectral density, $\langle ESD \rangle$, closer to the reference one; compare the $\langle ESD \rangle$ of the HP solution for $m = 200$ (red) and $m = 400$ (magenta) with the reference (black). The $\langle ESD \rangle$ of the modelled solution (blue) is much lower compared with that of the HP solution, especially for smaller scales.

4. Conclusions

In this study we have proposed to use the joint probability distribution (JPD) to probabilistically reconstruct the phase space which can be used when the original reference phase space (computed from numerical solutions, observations, or both) is too sparse to allow the use of data-driven methods. The probabilistically-reconstructed phase space is calculated by sampling from the JPD, thus providing an extra source of data from the reference distribution and ensuring that both the reference phase space and the reconstructed one share the same reference distribution. We have shown how the probabilistic reconstruction works on the example of Chua’s system and then successfully applied it within the context of the global ocean model NEMO.

The current methodology is limited to the phase space of HP solution computed in the probabilistically-reconstructed phase space. The phase space of HP solution is larger than the phase space computed from the data distribution (i.e. the probabilistically-reconstructed one), because the latter might have voids (which cannot be patched up by sampling from the JPD), while the former has no voids. Giving these limitations, the proposed methodology does allow us to compute the HP solution in the probabilistically-reconstructed (and reduced) phase space which is more accurate compared with the $1/4^\circ$ -NEMO simulation nonetheless. However, if the reference distribution changes over time (e.g. the reference solution drifts away from the phase space, used to compute the reference distribution) then the HP solution cannot follow these changes.

We have also found that the HP method can be used directly in reduced phase spaces thus allowing several-orders-of-magnitude acceleration (compared to the $1/4^\circ$ -resolution NEMO run), which can be translated into using larger ensemble of HP solutions for probabilistic predictions. Note that we compare only the degrees of freedom used in the HP method and those used in the NEMO model to get the solution at $1/4^\circ$ resolution. It goes without saying that the NEMO model evolves much more variables than the HP method, but in this comparison we pretend that NEMO needs only ~ 30000 grid points to compute the solution, while the HP method uses only 200 in the compressed phase space, and more importantly gives a solution which is closer to the reference one than that of the $1/4^\circ$ NEMO simulation.

We have studied how the proposed method performs on corrupted reference data (for which we considered three cases: randomly-missed states, gaps, and cuts) and found that the method works well even when sampling

from the JPD cannot patch up voids in the reference phase space. It allows us to conclude that the HP method in probabilistically-reconstructed phase spaces can be used as a fast reanalysis in which the complex dynamics of a comprehensive ocean model is replaced with the HP solution, as well as a dynamic interpolation method to stitch gaps in observational data.

The primary utility of the proposed methodology is to serve as a fast ocean, atmospheric, or ocean-atmospheric emulator in the reference phase space, or as an alternative to parameterisations in comprehensive ocean and ocean-atmospheric models. We believe that it demonstrates the strong potential and it can be of use in operational ocean and ocean-atmospheric models.

For studying climate change, one might think that the reference data set might be a limiting factor. And indeed, it is, but only if future climate states are not within the reference phase space. As it is a priori unknown whether future climate states are located in the reference phase space, one might consider using this methodology as an alternative to parameterisations in comprehensive models for near-term climate predictions (NTCP), instead of using it as a tool for forecasting, since more research is needed to address this question. Therefore, the next step in this direction would be to assess prediction skills and achievable forecast range of the method alone and in combination with high-resolution forecasting systems for NTCP.

Declaration of competing interest

The authors declare that they have no known competing financial interests or personal relationships that could have appeared to influence the work reported in this paper.

Data availability

The output of the global $1/4^\circ$ (ORCA025-N4001) and $1/12^\circ$ (ORCA0083-N006) resolution NEMO model used in this study is available on JASMIN (<https://jasmin.ac.uk/users/access/>) from these locations:

`/gws/nopw/j04/nemo_vol1/ORCA025-N401` and
`/gws/nopw/j04/nemo_vol1/ORCA0083-N006` .

Acknowledgments

The author thanks the Natural Environment Research Council for the support of this work through the projects CLASS and ATLANTIS (P11742-01), as well as Andrew Coward and Chris Wilson for the production of and help with the NEMO datasets, respectively.

References

- [1] M. Mendez, A. Ianiro, B. Noack, S. Brunton (Eds.), *Data-Driven Fluid Mechanics: Combining First Principles and Machine Learning*, Cambridge University Press, 2023.
- [2] H. V. Storch, F. Zwiers, *Statistical Analysis in Climate Research*, Cambridge Univ. Press, Cambridge, 2002.
- [3] E. Vanem, T. Zhu, A. Babanin, Statistical modelling of the ocean environment – A review of recent developments in theory and applications, *Marine Structures* 86 (2022).
- [4] L. Aguirre, C. Letellier, Modeling nonlinear dynamics and chaos: A review, *Mathematical Problems in Engineering* 2009 (2009) 1–35.
- [5] S. Brunton, J. Proctor, N. Kutz, Discovering governing equations from data by sparse identification of nonlinear dynamical systems, *PNAS* 113 (2016) 3932–3937.
- [6] S. Brunton, W. Brunton, J. Proctor, E. Kaiser, N. Kutz, Chaos as an intermittently forced linear system, *Nat. Commun.* 8 (2017) 1–9.
- [7] S. Mangiarotti, M. Huc, Can the original equations of a dynamical system be retrieved from observational time series?, *Chaos* 29 (2019) 023133.
- [8] I. Shevchenko, P. Berloff, A method for preserving nominally-resolved flow patterns in low-resolution ocean simulations: Constrained dynamics, *Ocean Model.* 178 (2022) 102098.
- [9] I. Shevchenko, D. Crisan, On energy-aware hybrid models, *JAMES* 16 (2024) e2024MS004306.

- [10] I. Shevchenko, P. Berloff, On a probabilistic evolutionary approach to ocean modelling: From Lorenz-63 to idealized ocean models, *Ocean Model.* 186 (2023) 102278.
- [11] T. Schneider, S. Lan, A. Stuart, J. Teixeira, Earth system modeling 2.0: A blueprint for models that learn from observations and targeted high-resolution simulations, *Geophys. Res. Lett.* 44 (2017).
- [12] S. Zhang, G. Lin, Robust data-driven discovery of governing physical laws with error bars, *P. Roy. Soc. A-Math. Phys. Eng.* 474 (2018).
- [13] P. O’Gorman, J. Dwyer, Using machine learning to parameterize moist convection: Potential for modeling of climate, climate change, and extreme events, *JAMES* 10 (2018).
- [14] L. Zanna, T. Bolton, Data-driven equation discovery of ocean mesoscale closures, *Geophys. Res. Lett.* 47 (2020).
- [15] J. Dramsch, Chapter one - 70 years of machine learning in geoscience in review, *Adv. Geophys.* 61 (2020) 1–55.
- [16] S. Brunton, B. Noack, P. Koumoutsakos, Machine learning for fluid mechanics, *Annu. Rev. Fluid Mech.* 52 (2020) 477–508.
- [17] Y. Ham, J. Kim, J. Luo, Deep learning for multi-year ENSO forecasts, *Nature* 573 (2019) 568–572.
- [18] K. Bi, L. Xie, H. Zhang, X. Chen, X. Gu, Q. Tian, Accurate medium-range global weather forecasting with 3D neural networks, *Nature* 619 (2023) 533–538.
- [19] D. Kochkov, J. Yuval, I. Langmore, et al., Neural general circulation models for weather and climate, *Nature* 632 (2024) 1060–1066.
- [20] A. Adadi, M. Berrada, Peeking Inside the Black-Box: A Survey on Explainable Artificial Intelligence (XAI), *IEEE Access* 6 (2018) 52138–52160.
- [21] C. Betancourt, T. T. Stomberg, A.-K. Edrich, A. Patnala, M. G. Schultz, R. Roscher, J. Kowalski, S. Stadtler, Global, high-resolution mapping of tropospheric ozone – explainable machine learning and impact of uncertainties, *Geoscientific Model Development* 15 (2022) 4331–4354.

- [22] I. Shevchenko, P. Berloff, A method for preserving large-scale flow patterns in low-resolution ocean simulations, *Ocean Model.* 161 (2021) 101795.
- [23] I. Shevchenko, P. Berloff, A method for preserving nominally-resolved flow patterns in low-resolution ocean simulations: Dynamical system reconstruction, *Ocean Model.* 170 (2022) 101939.
- [24] I. Shevchenko, P. Berloff, A hyper-parameterization method for comprehensive ocean models: Advection of the image point, *Ocean Model.* 184 (2023) 102208.
- [25] L. Devroye, *Non-Uniform Random Variate Generation*, Springer-Verlag, New York, Berlin, Heidelberg, Tokyo, 1986.
- [26] L. Sungbin, Y. Eun, B. Taehyun, K. Taewon, K. Seungwoo, L. Kyungjae, C. Sungjoon, Score-based generative modeling through stochastic evolution equations in hilbert spaces, in: A. Oh, T. Naumann, A. Globerson, K. Saenko, M. Hardt, S. Levine (Eds.), *Advances in Neural Information Processing Systems*, Vol. 36, Curran Associates, Inc., 2023, pp. 37799–37812.
- [27] L. Chua, M. Komuro, T. Matsumoto, *IEEE Transactions on Circuits and Systems* 33 (1986) 1072–1118.
- [28] R. Preisendorfer, *Principal Component Analysis in Meteorology and Oceanography*, Elsevier, 1988.
- [29] J. Chambers, T. Hastie (Eds.), *Statistical models in S*, Chapman & Hall, 1992.